Chiral critical behavior of 3D lattice fermionic models with quartic interactions

Claudio Bonati,[1] Alessio Franchi,[1] Andrea Pelissetto,[2] and Ettore Vicari[1]
[1]Dipartimento di Fisica dell'Università di Pisa and INFN, Largo Pontecorvo 3, I-56127 Pisa, Italy
[2]Dipartimento di Fisica dell'Università di Roma Sapienza and INFN Sezione di Roma I, I-00185 Roma, Italy

(Received 2 January 2023; accepted 31 January 2023; published 22 February 2023)

We study the critical behavior of the three-dimensional Gross-Neveu (GN) model with N_f four-component Dirac fermionic flavors and quartic interactions, at the chiral $\mathbb{Z}_2$ transition in the massless $\mathbb{Z}_2$-symmetric limit. For this purpose, we consider a lattice GN model with staggered Kogut-Susskind fermions and a scalar field coupled to the scalar bilinear fermionic operator, which effectively realizes the attractive four-fermion interaction. We perform Monte Carlo simulations for $N_f = 4$, 8, 12, 16. By means of finite-size scaling analyses of the numerical data, we obtain estimates of the critical exponents, which are compared with the large-N_f predictions obtained using the continuum GN field theory. We observe a substantial agreement. This confirms that lattice GN models with staggered fermions provide a nonperturbative realization of the GN quantum field theory, even though the lattice interactions explicitly break the flavor $\mathrm{U}(N_f) \otimes \mathrm{U}(N_f)$ symmetry of the GN field theory, which is only recovered in the critical limit.

DOI: 10.1103/PhysRevD.107.034507

I. INTRODUCTION

Three-dimensional (3D) quantum field theories (QFTs) of interacting fermions emerge in different contexts; for instance, in condensed-matter physics, they are used to describe the low-energy excitations in graphene, see, e.g., Refs. [1–9]. Among them, we should mention quantum electrodynamics with charged fermions, the Gross-Neveu and the Gross-Neveu-Yukawa models, in which the dynamics of Dirac fermions arises from four-fermion interaction terms or through the coupling with a scalar field [10].

In this paper, we focus on the Gross-Neveu (GN) QFT defined by the Euclidean Lagrangian density

$$\mathcal{L} = -\sum_{f=1}^{N_f} \bar{\Psi}_f (\not{\partial} + m) \Psi_f - \frac{g^2}{2N_f} \left(\sum_{f=1}^{N_f} \bar{\Psi}_f \Psi_f \right)^2, \quad (1)$$

where $\Psi_f(\boldsymbol{x})$ with $f = 1, \ldots, N_f$ is a fermionic field. Each *flavor* component Ψ_f is a four-dimensional spinor, so that the total number N of fermionic components is given by $N = 4N_f$, and the matrices γ_μ are the usual Euclidean 4×4 matrices used in 4 dimensions [11]. This choice allows us to define chiral symmetry transformations [12]. It is also somehow necessary if we wish to compare our findings with ϵ-expansion ($\epsilon = 4 - d$) results obtained in the four-dimensional model with standard Dirac spinors [13]. Note that in three dimensions it is also possible to define GN QFTs with two-component spinors: in this case no chirality is present, but an analogous role is played by the reflection with respect to one of the axes [10,14]. The Lagrangian in Eq. (1), with attractive four-fermion interactions, can be equivalently written as

$$\mathcal{L} = -\sum_{f=1}^{N_f} \bar{\Psi}_f (\not{\partial} + m + \Phi) \Psi_f + \frac{N_f}{2g^2} \Phi^2, \quad (2)$$

where $\Phi(\boldsymbol{x})$ is an auxiliary real scalar field associated with the bilinear fermionic operator $\sum_f \bar{\Psi}_f \Psi_f$. Indeed, by integrating out the scalar field Φ, one recovers Lagrangian (1).

The global flavor symmetry of the GN QFT is $\mathrm{U}(N_f) \otimes \mathrm{U}(N_f)$ [11,13]. If fermions are massless, the 3D Lagrangian is also invariant under two additional $\mathbb{Z}_2$ chiral transformations [11,13]

$$\begin{aligned} &\Psi_f \to \gamma_5 \Psi_f, \qquad \bar{\Psi}_f \to -\bar{\Psi}_f \gamma_5, \qquad \Phi \to -\Phi, \\ &\Psi_f \to \gamma_4 \Psi_f, \qquad \bar{\Psi}_f \to -\bar{\Psi}_f \gamma_4, \qquad \Phi \to -\Phi. \end{aligned} \quad (3)$$

The presence of two chiral symmetries is related to the fact that only the γ_μ matrices with $\mu = 1$, 2, 3 appear in the Lagrangian, so that γ_4 and γ_5 play essentially the same role [13]. In the massless GN models with attractive interactions and at least for a sufficiently large number of flavors [14], there is a phase transition where the chiral

Published by the American Physical Society under the terms of the Creative Commons Attribution 4.0 International license. Further distribution of this work must maintain attribution to the author(s) and the published article's title, journal citation, and DOI. Funded by SCOAP[3].

$\mathbb{Z}_2$ symmetries are spontaneously broken. This transition separates a disordered phase, in which the scalar-field correlations are short ranged and fermions are massless, from an ordered phase, in which the scalar field orders (in field-theory terms, it has a nonvanishing expectation value), providing an effective mass for the fermion fields. As discussed in Refs. [10,14], a similar behavior is expected in the Gross-Neveu-Yukawa (GNY) QFT, which is an extension of the GN model obtained by adding a kinetic and a quartic-interaction term for the real scalar field.

The massless GN QFT with attractive interactions should provide the effective description of the critical behavior of systems with the same global symmetry, symmetry-breaking pattern and field content. In the case of the GN model, the symmetry that is broken is always the chiral $\mathbb{Z}_2 \otimes \mathbb{Z}_2$ symmetry, for any N_f. Therefore, the relevant symmetry and symmetry-breaking pattern at the transition are always the same. However, the resulting critical behavior depends on N_f, because of the different fermion content of the model. Indeed, the chiral transition occurs in the presence of N_f massless fermions, which generate long-range interactions for the scalar field, which obviously depend on N_f.

The renormalization-group (RG) flow in the GN and GNY QFTs has been investigated using different methods. Critical exponents have been computed in the d-dimensional theory in the large-N_f limit. Results to order $1/N_f^2$ are reported in Refs. [14–21]. They provide quantitative information that can be compared with results obtained in statistical models that, supposedly, have transitions associated with these QFTs. The RG flow has also been studied in perturbation theory. Perturbative calculations have been performed around four dimensions in the GNY model [22] to four loops, providing the ϵ expansions of the critical exponents up to $O(\epsilon^4)$. *A priori*, it is not clear if these results directly apply to the three-dimensional model. Indeed, in the four-dimensional model the Lagrangian is invariant under a single chiral symmetry—the chiral symmetry group is $\mathbb{Z}_2$—while in three dimensions the chiral symmetry group is larger, being $\mathbb{Z}_2 \otimes \mathbb{Z}_2$. However, the large-$N_f$ expressions of the critical exponents do not show nonanalyticities as $d \to 3$, indicating that this dimension-dependent symmetry enlargement should have no impact on the d-dependent analyticity properties of the universal features of the model. We should also remark that ϵ expansions for the GNY model are not Borel summable, at variance with what happens for the corresponding expansions in Φ^4 scalar theories, see, e.g., Refs. [10,23,24]. Therefore, we do not expect them to provide accurate 3D estimates. A thorough analysis of the perturbative series is reported in Ref. [25]. Exponents have also been computed using the functional renormalization group [26] and the conformal-bootstrap approach [27,28].

Numerical results [29–36] for relatively small values of N_f, i.e., for $N_f \leq 4$, have been compared with the estimates obtained in the field-theory approaches (see, e.g., the results reported in Table 3 of Ref. [27], where $N = 4N_f$). In some cases, large discrepancies are observed among the results obtained [for instance, for $N_f = 1$, the estimates of $1/\nu$ vary between 0.76 and 1.30(5)]. In particular, the conformal-bootstrap results of Ref. [27], which have been recently confirmed in Ref. [28], provide estimates that differ significantly from those obtained using numerical methods. This uncertain situation calls for further studies, to understand the reasons of such discrepancies, whether QFT correctly predicts the universal features of the critical transitions of the corresponding statistical lattice systems.

In this paper we investigate the critical behavior of 3D statistical fermionic models defined on cubic lattices, to shed light on the way, or whether, they realize the continuum GN QFT at the chiral transition. The definition of fermionic lattice models is affected by the well-known fermion doubling problem [37,38], which makes it impossible to implement the quartic fermion interaction, or, equivalently, the interaction between fermionic and scalar fields, preserving the flavor symmetry $\mathrm{U}(N_f) \otimes \mathrm{U}(N_f)$. A partial solution is provided by Kogut-Susskind (KS) formulations [15,38]. In this case, two doublers are present in the model, so that $N_f/2$ KS fermion variables per site are needed to describe a system with N_f flavors. In these models the Hamiltonian is only exactly invariant under $\mathrm{U}(N_f/2)$ global transformations and, in the massless limit, under a single $\mathbb{Z}_2$ chiral symmetry. If the scalar-field variables are located on the dual lattice sites [15,38], the terms that break the symmetry between the doublers, and therefore the full flavor symmetry of the continuum model, are $O(a)$ (a is the lattice spacing) in the formal *classical* continuum $a \to 0$ limit. Therefore, the symmetry $\mathrm{U}(N_f) \otimes \mathrm{U}(N_f)$ of the continuum GN and GNY models is recovered at the leading *classical* tree order. In the RG context, this result is taken as an indication that these breaking terms are irrelevant perturbations of the GNY QFT fixed point, so that the lattice systems recover the continuum $\mathrm{U}(N_f) \otimes \mathrm{U}(N_f)$ symmetry at the chiral transition point. Thus, their asymptotic critical behavior belongs to the same universality class as that of the continuum QFT of GN and GNY models.

Here we return to this issue, verifying whether the conjectured irrelevance of the $O(a)$ flavor-symmetry violations holds at the chiral transition of 3D lattice GN models. Indeed, although the fact that the flavor-symmetry violating terms are $O(a)$ is generally required to recover the full flavor symmetry, it may not be sufficient at a nonperturbative level. Therefore, an accurate check at a nonperturbative level is called for, performed by carefully studying the critical behavior at the chiral transition. For this purpose, we focus on the large-N_f regime and compare Monte Carlo (MC) results with the available nonperturbative large-N_f expansions of the critical exponents computed using the GN QFT. Since the critical behavior in the

$N_f \to \infty$ limit of lattice models matches that of the continuum GN models [15], we focus on the $O(N_f^{-1})$ corrections, which depend on the actual number of flavor components.

In our numerical simulations we use the KS staggered formulation of Ref. [15], with scalar fields located at the sites of the dual lattice. To compare with the large-N_f predictions obtained for the GN QFT (1), we perform simulations for $N_f = 4$, 8, 12, 16, and present numerical finite-size scaling (FSS) analyses. We anticipate that our numerical results for the critical behavior of the lattice KS formulation agree with the available large-N_f QFT results. Thus, they support the conjectured identification of the GN QFT as the effective model for the critical behavior of lattice GN systems.

The paper is organized as follows. In Sec. II we present the lattice KS formulation of the GN model that we consider. Section III outlines the strategy of our analysis of the numerical data. In Sec. IV we report the large-N_f expansions of the critical exponents, which are then compared with numerical results. Section V is devoted to the presentation of the numerical results for various flavor numbers, i.e., $N_f = 4$, 8, 12, 16. Finally, in Sec. VI we summarize and draw our conclusions. In the appendices we report a discussion of the relation between the fermionic condensate and the scalar field, some technical details on the simulations, and a collection of FSS results.

II. LATTICE FORMULATIONS

A *naive* lattice formulation of the 3D massless GN model (1) can be obtained by discretizing the Lagrangian density (2) on a cubic lattice. The lattice Hamiltonian is [38]

$$H_N = \sum_{\boldsymbol{x},\mu,c} \bar{\psi}^c_{\boldsymbol{x}} (\gamma_\mu \Delta_\mu + \sigma_{\boldsymbol{x}}) \psi^c_{\boldsymbol{x}} + \frac{1}{2g^2} \sum_{\boldsymbol{x}} \sigma^2_{\boldsymbol{x}}, \tag{4}$$

where $c = 1, \ldots, N_\psi$ and $\mu = 1$, 2, 3. Here, $\psi^c_{\boldsymbol{x}}$ is a four-component spinor for each value of the flavor index c, γ_μ are the four-dimensional γ matrices, and $\Delta_\mu \psi^c_{\boldsymbol{x}} = (\psi^c_{\boldsymbol{x}+\hat{\mu}} - \psi^c_{\boldsymbol{x}-\hat{\mu}})/2$. We set the lattice spacing $a = 1$. One can easily verify that model (4), as the massless GN model (2), is invariant under two *chiral* $\mathbb{Z}_2$ symmetries:

$$\begin{aligned} &\psi^c_{\boldsymbol{x}} \to \gamma_5 \psi^c_{\boldsymbol{x}}, \qquad \bar{\psi}^c_{\boldsymbol{x}} \to -\bar{\psi}^c_{\boldsymbol{x}} \gamma_5, \qquad \sigma_{\boldsymbol{x}} \to -\sigma_{\boldsymbol{x}}, \\ &\psi^c_{\boldsymbol{x}} \to \gamma_4 \psi^c_{\boldsymbol{x}}, \qquad \bar{\psi}^c_{\boldsymbol{x}} \to -\bar{\psi}^c_{\boldsymbol{x}} \gamma_4, \qquad \sigma_{\boldsymbol{x}} \to -\sigma_{\boldsymbol{x}}, \end{aligned} \tag{5}$$

which protect the fermion field against the generation of a mass term. Moreover, the model (4) is invariant under the global symmetry group $\mathrm{U}(N_\psi) \otimes \mathrm{U}(N_\psi)$.

The above model does not have the exact flavor content of the GN field theory due to the lattice fermion doubling. Indeed, the Hamiltonian (4) actually describes $8N_\psi$ massless flavors in the formal continuum limit $a \to 0$. They are associated with the Fourier-transform components with $k_\mu = 0$ and $k_\mu = \pi/a$ along each direction. However, the scalar-field interaction breaks the symmetry of the doublers and therefore this lattice formulation does not describe $N_f = 8N_\psi$ identical flavors as required by the GN model, but N_f massless flavors with complex self-interactions that do not reproduce the field-theory model with Lagrangian density (2) in the classical continuum limit $a \to 0$. As put forward in Refs. [15,38], the problem can be attenuated by defining the scalar fields on the dual lattice, i.e., at the center of the lattice cubes, located at

$$\tilde{\boldsymbol{x}} = \boldsymbol{x} + \sum_\mu \hat{\mu}/2, \tag{6}$$

where $\hat{\mu}$ are the unit vectors associated with the lattice directions. The Hamiltonian (4) is replaced by

$$H_D = \sum_{\boldsymbol{x},\mu,c} \bar{\psi}^c_{\boldsymbol{x}} \left(\gamma_\mu \Delta_\mu + \frac{1}{8} \sum_{\langle \boldsymbol{x}, \tilde{\boldsymbol{x}} \rangle} \sigma_{\tilde{\boldsymbol{x}}} \right) \psi^c_{\boldsymbol{x}} + \frac{1}{2g^2} \sum_{\tilde{\boldsymbol{x}}} \sigma^2_{\tilde{\boldsymbol{x}}}, \tag{7}$$

where the second term includes a sum over the eight sites $\langle \boldsymbol{x}, \tilde{\boldsymbol{x}} \rangle$ of the dual lattice surrounding $\boldsymbol{x}$. Following Ref. [38], one can show that the global flavor symmetry for all $N_f = 8N_\psi$ flavors is recovered at the classical tree-order level: in the formal expansion of the Hamiltonian in powers of a, the terms breaking the flavor symmetry are of order a in the $a \to 0$ limit. Therefore, at least in the classical limit, apart from $O(a)$ corrections, one effectively recovers the $\mathrm{U}(N_f) \otimes \mathrm{U}(N_f)$ symmetry with $N_f = 8N_\psi$. The Hamiltonian (7) is also exactly invariant under chiral $\mathbb{Z}_2$ symmetry transformations. They are defined as in Eq. (5) with $\sigma_{\boldsymbol{x}}$ replaced by $\sigma_{\tilde{\boldsymbol{x}}}$. We also mention that alternative implementations of lattice GN models with *naive* fermions, also providing the correct $a \to 0$ limit, have been discussed and numerically investigated in Refs. [39,40].

To reduce the problem of fermionic doubling, one can consider the staggered KS formulation. For 3D systems defined on cubic lattices, there are only two doublers instead of the eight ones appearing in the naive formulation. By using N_χ staggered fermionic fields $\chi^c_{\boldsymbol{x}}$, we obtain a lattice formulation with $N_f = 2N_\chi$ effective massless flavors. The partition function is [15]

$$Z = \int [\mathrm{d}\chi \mathrm{d}\bar{\chi}] [\mathrm{d}\sigma] e^{-H_S[\bar{\chi},\chi,\sigma]}, \tag{8}$$

$$H_S = \sum_{\boldsymbol{x},\boldsymbol{y},c} \bar{\chi}^c_{\boldsymbol{x}} M_{\boldsymbol{x},\boldsymbol{y}} \chi^c_{\boldsymbol{y}} + \frac{\kappa N_\chi}{2} \sum_{\tilde{\boldsymbol{x}}} \sigma^2_{\tilde{\boldsymbol{x}}}, \tag{9}$$

where $\chi^c_{\boldsymbol{x}}$ is defined on the sites $\boldsymbol{x}$ of the cubic lattice (the index c runs from 1 to N_χ), $\sigma_{\tilde{\boldsymbol{x}}}$ is a real scalar field on the dual lattice site $\tilde{\boldsymbol{x}}$, and κ is the model parameter that is tuned to approach the critical point [15]. The matrix M is given by

$$M_{x,y}(\sigma) = \sum_{\mu} \frac{\eta_\mu(x)}{2} (\delta_{y,x+\hat{\mu}} - \delta_{y,x-\hat{\mu}}) + \frac{1}{8} \sum_{\langle x,\tilde{x}\rangle} \sigma_{\tilde{x}} \delta_{x,y}. \quad (10)$$

In the above expression, the second sum is over the sites of the dual lattice that surround x, and $\eta_\mu(x)$ is the Kawamoto-Smit phase $\eta_\mu(x) = (-1)^{x_1+..+x_{\mu-1}}$. The matrix $M_{x,y}$ satisfies the relation

$$M_{x,y}(-\sigma) = -M_{y,x}(\sigma). \quad (11)$$

Apart from irrelevant normalization constants, by integrating out the fermionic variables we obtain the partition function

$$Z = \int [d\sigma] [\det M_{x,y}(\sigma)]^{N_\chi} \exp\left(-\frac{\kappa N_\chi}{2} \sum_{\tilde{x}} \sigma_{\tilde{x}}^2\right). \quad (12)$$

The staggered KS formulation (9) maintains an exact *chiral* $\mathbb{Z}_2$ symmetry, corresponding to

$$\chi_x^c \to P_x \chi_x^c, \qquad \bar{\chi}_x^c \to -P_x \bar{\chi}_x^c, \qquad \sigma_{\tilde{x}} \to -\sigma_{\tilde{x}}, \quad (13)$$

where $P_x = (-1)^{\sum_i x_i}$ is the parity of the site x.

As in the naive fermion formulation, the continuum flavor symmetry $\mathrm{U}(N_f) \otimes \mathrm{U}(N_f)$ of the continuum GN field theory is not exact. The exact flavor-symmetry group of the lattice model is only $\mathrm{U}(N_\chi)$, where $N_\chi = N_f/2$. However, as shown in Ref. [15], in the formulation (9) with scalar fields on the dual lattice, the symmetries of the continuum GN field theory are recovered in the formal classical limit $a \to 0$. Violations are of order a and vanish in the formal continuum limit.

III. FINITE-SIZE SCALING AT THE CHIRAL TRANSITION

We investigate numerically the critical behavior of the lattice KS formulation, using FSS methods applied to several observables defined in terms of the scalar and fermionic fields. In our work boundary conditions (BC) have been chosen as follows. For fermionic fields we use antiperiodic BC in one of the directions (we have chosen the third direction, $\mu = 3$) and periodic BC in the other ones. For the scalar field $\sigma_{\tilde{x}}$ we use periodic BC in all directions.

A. Observables

We define the two-point function of the $\sigma_{\tilde{x}}$ field as

$$G_\sigma(\tilde{x} - \tilde{y}) = \langle \sigma_{\tilde{x}} \sigma_{\tilde{y}} \rangle \quad (14)$$

(it only depends on $\tilde{x} - \tilde{y}$ because of the translation invariance preserved by the periodic BC) and the corresponding Fourier transform $\tilde{G}_\sigma(p) = \sum_{\tilde{x}} e^{ip\cdot\tilde{x}} G_\sigma(\tilde{x})$. The scalar susceptibility χ_σ and second-moment correlation length ξ_σ are defined as

$$\chi_\sigma = \tilde{G}_\sigma(0), \quad (15)$$

$$\xi_\sigma^2 = \frac{1}{4\sin^2(p_m/2)} \frac{\tilde{G}_\sigma(0) - \tilde{G}_\sigma(p_m)}{\tilde{G}_\sigma(p_m)}, \quad (16)$$

where $p_m \equiv (0, 0, 2\pi/L)$ (the third direction is the one in which we use antiperiodic BC for the fermionic variables). We also consider the space average of the scalar order parameter

$$\Sigma = \frac{1}{V} \sum_{\tilde{x}} \sigma_{\tilde{x}} \quad (17)$$

(note that $\langle \Sigma \rangle = 0$ because of the chiral symmetry), and the corresponding Binder parameters

$$U_4 = \frac{\langle \Sigma^4 \rangle}{\langle \Sigma^2 \rangle^2}, \qquad U_2 = \frac{\langle \Sigma^2 \rangle}{\langle |\Sigma|^2 \rangle}. \quad (18)$$

The observables U_4, U_2, and $R_\xi \equiv \xi_\sigma/L$, are RG invariant at the transition where the scalar-field and fermionic correlations are critical. They will play a central role in our numerical FSS analyses.

We define the fermionic susceptibility χ_χ as

$$\chi_\chi \equiv \frac{1}{V} \langle |\sum_{x,y} \bar{\chi}_x^c \chi_y^c| \rangle = \frac{1}{V} \langle |\sum_{x,y} M_{x,y}^{-1}| \rangle. \quad (19)$$

The absolute value in Eq. (19) is required by the presence of the $\mathbb{Z}_2$ invariance. Indeed, using Eq. (11) one can easily prove that $\langle \sum_{x,y} M_{x,y}^{-1} \rangle$ vanishes.

We also consider the fermionic bilinear $\sum_c \bar{\chi}_x^c \chi_x^c$ and its space average

$$\Xi = \frac{1}{V} \sum_c \sum_x \bar{\chi}_x^c \chi_x^c. \quad (20)$$

Because of the chiral $\mathbb{Z}_2$ symmetry

$$\langle \Xi \rangle = \frac{1}{V} \langle \mathrm{Tr}\, M^{-1} \rangle = 0. \quad (21)$$

The average value of higher powers of Ξ can be directly related to averages of the scalar order parameter Σ. Indeed, in the infinite-volume limit, see Appendix A, we have

$$\langle \Xi^n \rangle = \kappa^n N_\chi^n \langle \Sigma^n \rangle. \quad (22)$$

More generally, see Appendix A, the correlations of the scalar variable $\sigma_{\tilde{x}}$ and of the fermionic bilinear $\sum_c \bar{\chi}_x^c \chi_x^c$ are directly related, apart from contact terms. This relation expresses the equivalence of the scalar field σ and of the

bilinear $\bar{\chi}\chi$ operator. The presence of contact terms is not unexpected, because of the different nature of the two quantities. For instance, $(\bar{\chi}\chi)^{N_\chi}$ vanishes because of the Grassmannian nature of the variables, while obviously σ^{N_χ} is nonvanishing.

B. FSS strategy to determine the critical exponents

We now present the FSS relations we will use in the numerical analysis. To estimate the correlation-length exponent ν and the critical value κ_c, we analyze the behavior of RG invariant quantities R (such as U_4, U_2, and $R_\xi \equiv \xi_\sigma/L$, defined in Sec. III A). Close to the critical point $\kappa = \kappa_c$, they are expected to behave as

$$R(\kappa, L) \approx \mathcal{R}(X), \qquad X = (\kappa - \kappa_c) L^{1/\nu}, \tag{23}$$

in the large-L FSS limit. The function $\mathcal{R}(X)$ is universal up to a multiplicative rescaling of its argument. In particular, $R^* \equiv \mathcal{R}(0)$ is universal, depending only on the boundary conditions and aspect ratio of the lattice. Equation (23) holds up to scaling corrections, decaying as $L^{-\omega_l}$, where $\omega_l > 0$ is the leading scaling-correction exponent.

If a RG invariant quantity $\hat{R}$ is a monotonic function of X—this is the case of the ratio $R_\xi = \xi_\sigma/L$—in the FSS limit we can express a different RG invariant quantity R as a function of $\hat{R}$ simply as

$$R(\kappa, L) = F_R(\widehat{R}) + O(L^{-\omega_l}), \tag{24}$$

where $F_R(x)$ depends only on the universality class, boundary conditions and lattice shape, without nonuniversal multiplicative factors. Scaling (24) is particularly convenient to test universality-class predictions, since it permits easy comparisons between different models without requiring the tuning of nonuniversal parameters. FSS analyses based on Eq. (24) have been recently exploited to characterize the universality classes of two- and three-dimensional lattice models, including systems with gauge symmetries, such as Abelian Higgs models and scalar chromodynamics, see, e.g., Refs. [41–45].

Another independent critical exponent is η_σ. It can be defined in terms of the critical behavior of the two-point function G_σ defined in Eq. (14). In the thermodynamic limit and at the critical point, $G_\sigma(z)$ behaves as

$$G_\sigma(z) \sim |z|^{-2y_\sigma}, \tag{25}$$

where $y_\sigma = (d - 2 + \eta_\sigma)/2$ is the RG dimension of the scalar field σ. The exponent η_σ can be estimated from the FSS behavior of the scalar susceptibility χ_σ defined in Eq. (15), which is expected to scale as

$$\chi_\sigma(\kappa, L) \approx L^{2-\eta_\sigma} \mathcal{S}(X), \tag{26}$$

where $\mathcal{S}$ is a universal function apart from an overall factor and a rescaling of the argument. We can also replace X with a monotonic RG invariant quantity $\widehat{R}$, as

$$\chi_\sigma(\kappa, L) \approx L^{2-\eta_\sigma} F_\sigma(\widehat{R}), \tag{27}$$

where $F_\chi(\widehat{R})$ is universal apart from a multiplicative factor only. The critical exponent η_f, related to the RG dimension of the fermionic field $y_\psi = (d - 1 + \eta_f)/2$, can be obtained from the analysis of the fermionic susceptibility χ_χ defined in Eq. (19). In the FSS limit, it satisfies the scaling relation

$$\chi_\chi(\kappa, L) \approx L^{1-\eta_f} F_\chi(\widehat{R}). \tag{28}$$

IV. LARGE-N_f RESULTS WITHIN QFT

In this section, we report the known leading terms of the large-N_f expansion of the exponents ν, η_σ, and η_f defined in the previous section. They are given by [14,18,19,28]

$$\frac{1}{\nu} \approx 1 - \frac{8}{3\pi^2} N_f^{-1} + \frac{4(27\pi^2 + 632)}{27\pi^4} N_f^{-2}, \tag{29}$$

$$\eta_\sigma \approx 1 - \frac{16}{3\pi^2} N_f^{-1} - \frac{4(27\pi^2 - 304)}{27\pi^4} N_f^{-2}, \tag{30}$$

$$\eta_f \approx \frac{2}{3\pi^2} N_f^{-1} + \frac{122}{27\pi^4} N_f^{-2} + \frac{4}{27\pi^6} \left(\frac{47\pi^2}{12} + 9\pi^2 \ln 2 - \frac{189}{2} \zeta(3) - \frac{167}{9} \right) N_f^{-3}. \tag{31}$$

The $1/N_f$ expansion allows us to predict also the exponents of the scaling corrections. First, there are scaling corrections related to the irrelevant fields that appear in the continuum GN QFT. The correspondent leading scaling-correction exponent is [21]

$$\omega = 1 - \frac{32}{3\pi^2} N_f^{-1}. \tag{32}$$

There are also scaling corrections that are specific of the lattice model. The most relevant ones are associated with the operator that breaks the flavor symmetry. Since this term is formally of order a in the continuum tree-level approximation [15], we can predict that the corresponding correction-to-scaling exponent ω_d is 1 for $N_f \to \infty$, i.e.,

$$\omega_d = 1 + O(N_f^{-1}). \tag{33}$$

The exponents defined in Eqs. (32) and (33) coincide for $N_f = \infty$. For finite values of N_f, they differ (we do not know which one is the smallest), but, if N_f is large, they should be still close enough to justify the use of a single correction to scaling with exponent $\omega \approx 1$. For small values

of N_f their difference might be significant. In this case, the presence of two different correction terms would make the numerical analysis quite challenging.

It is important to stress that the large-N_f expansions reported above refer to the model (1) and four-dimensional spinors (therefore, the total number of fermionic-field components is $4N_f$). This model is equivalent to the one in which two-dimensional spinors are used and γ^1, γ^2, and γ^3 are identified with the Pauli matrices. More precisely, expectation values of the scalar field σ in the model with N_f four-dimensional spinors are the same as in the model with $2N_f$ two-dimensional spinors [39]. Therefore, the large-N_f expansions also hold in the latter model, provided N_f is replaced by $N_f/2$.

We finally mention that the critical value κ_c for the KS formulation (9) was computed in the limit $N_\chi \to \infty$, obtaining [15,46,47]

$$\kappa_{c,\infty} = 2\int_0^\infty dz\, e^{-3z} I_0^3(z) = \frac{(\sqrt{3}-1)\Gamma(\frac{1}{24})^2\Gamma(\frac{11}{24})^2}{48\pi^3} \tag{34}$$

where I_0 is the modified Bessel function. Numerically, we find $\kappa_{c,\infty} = 1.010924039\ldots$

V. NUMERICAL ANALYSES

We now outline our numerical FSS analyses of the MC data. We simulate the staggered KS model (9) using the hybrid MC algorithm, see Appendix B for technical details. We present results for various numbers of massless flavors, i.e., for $N_f = 4$, 8, 12, 16, to check the approach to the large-N_f limit. They correspond to $N_\chi = 2$, 4, 6, 8 equal staggered components χ^c_x. Even numbers of N_χ are required to avoid the sign problem in the MC simulations, see Appendix B.

The efficiency of the hybrid MC algorithms for fermionic models significantly decreases when increasing the size of the lattice: autocorrelation times generally increase with a large power of L [48]. The computational cost in our MC simulations appears to approximately increase as L^6 in the critical region, see Appendix B for some details. For this reason, we performed simulations on relatively small lattices, up to $L \approx 40$, where it was possible to obtain accurate data. Obtaining precise estimates for bigger lattices would require a much larger numerical effort. We also mention that our MC simulations took about 10^2 years of CPU-time on a single core of a standard processor.

The FSS analysis of the MC data shows clear evidence of a continuous chiral transition for all values of N_f considered. The MC estimates of the RG invariant quantities R_ξ, U_4, U_2 defined Sec. III A, show a clear crossing point; see, e.g., Fig. 1, where we report R_ξ as a function of κ for $N_f = 8$.

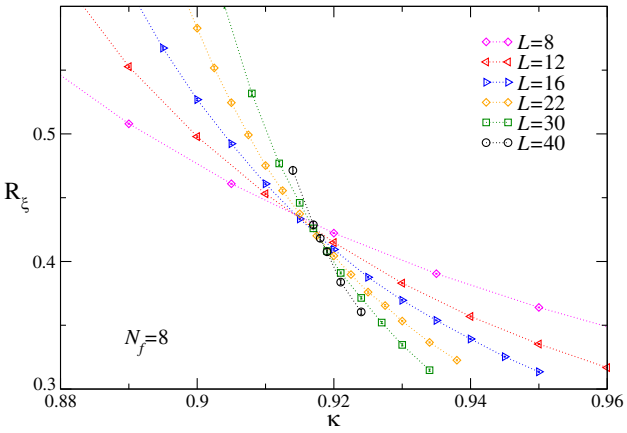

FIG. 1. MC estimates of R_ξ versus κ for $N_f = 8$. The data for different lattice sizes have a crossing point for $\kappa_c \approx 0.92$. The lines correspond to linear interpolations and are drawn just to guide the eye.

To determine the critical point κ_c and the exponent ν, we fitted R_ξ, U_4, and U_2 to the general FSS relation (23). We performed fits parametrizing $\mathcal{R}(X)$ with a polynomial in X, including only data satisfying $L \geq L_{\rm min}$, to identify scaling corrections. We also performed combined fits of pairs of observables to

$$R(\kappa, L) = \mathcal{R}(X) + L^{-\omega_l}\mathcal{R}_c(X), \tag{35}$$

fixing $\omega_l = 1$ (this should be a reasonable estimate for N_f large, as discussed in Sec. IV). The results show some tiny trends both for κ_c and ν and also some dependence on the observable considered. Scaling corrections, numerically large compared to our tiny error bars, are clearly present. As an example, we report the estimates of κ_c for $N_f = 12$, obtained from the analysis of the data in the range $-0.3 \leq X \leq 0.3$. The analysis of R_ξ provides $\kappa_c = 0.9463(1), 0.9470(1)$, for $L_{\rm min} = 12$ and 16, respectively. The analysis of U_4 gives instead $\kappa_c = 0.9472(1)$, $0.9479(3)$. It is clear that the statistical error is negligible compared with the systematic error due to the scaling corrections. If we consider the differences of these numbers as an estimate of the systematic uncertainty, we end up with $\kappa_c = 0.9627(7), 0.9475(6), 0.9180(5)$, $0.8348(8)$ for $N_f = 16$, 12, 8, 4, respectively. Our result for $N_f = 4$ is in agreement with the estimate reported in Ref. [29], $\kappa_c = 0.835(1)$.

The estimates of κ_c appear to approach the $N_f \to \infty$ critical value $\kappa_{c,\infty} \approx 1.0109$ with increasing N_f, cf. Eq. (34), as shown in Fig. 2. Actually, they appear to converge to the $N_f = \infty$ critical value as

$$\kappa_c(N_f) = \kappa_{c,\infty} + a_1 N_f^{-1} + O(N_f^{-2}) \tag{36}$$

with $a_1 \approx -0.8$.

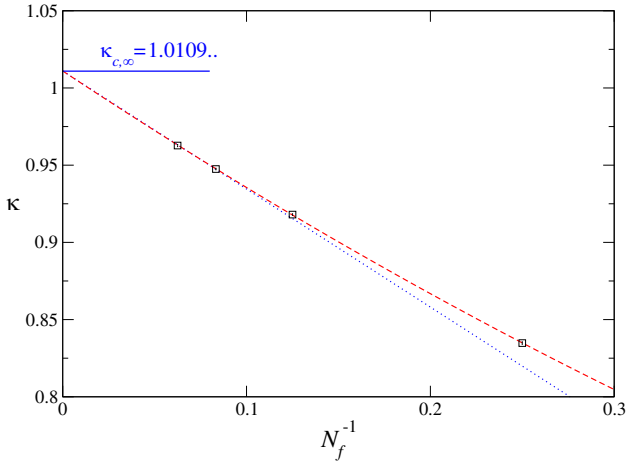

FIG. 2. Estimates of the critical value κ_c versus N_f^{-1}. They are fully consistent with the behavior $\kappa_c(N_f) = \kappa_{c,\infty} + a_1 N_f^{-1}$, where $\kappa_{c,\infty} \approx 1.0109$ is the exact result for $N_f = \infty$, see Eq. (36). The blue dotted line corresponds to $\kappa_c(N_f) = \kappa_{c,\infty} + a_1 N_f^{-1}$; a fit of the data with $N_f = 12$ and 16 gives $a_1 = -0.764(4)$. The red dashed line corresponds to $\kappa_c(N_f) = \kappa_{c,\infty} + a_1 N_f^{-1} + a_2 N_f^{-2}$, where the coefficients were obtained by fitting all data (χ^2/d.o.f. ≈ 0.4): $a_1 = -0.788(4)$ and $a_2 = 0.33(2)$.

The same fits that determine κ_c provide estimates of the critical exponent ν. They are reported in Table I. Again the error takes into account the small differences obtained from the analyses of R_ξ, U_4, and U_2. Also for ν, the differences among the estimates obtained by analyzing the different observables are larger than the statistical error of the fits, indicating the presence of scaling corrections somehow larger than the statistical errors. As an example we report the results for $N_f = 12$ (the corresponding estimates of κ_c are reported above). For $L_{\min} = 12, 16$ we obtain $\nu = 1.027(5)$, 1.04(1) from the analysis of R_ξ, and $\nu = 1.01(1)$, 1.00(1), from the analysis of U_4, which are somewhat inconsistent at the level of the (relatively small) statistical errors. The final estimates of ν are in good agreement with the estimates (column LN in Table I) obtained by using the large-N_f expansion (29) to order N_f^{-2}. As an example of the quality

TABLE I. Estimates of the universal critical exponents ν, η_σ and η_f, obtained in this paper (MC). We also report the large-N_f estimates (LN) obtained using the expansions Eqs. (29)–(31). For the exponent ν we used the direct expansion to order N_f^{-2}, obtained by inverting Eq. (29).

	ν		η_σ		η_f	
N_f	MC	LN	MC	LN	MC	LN
16	1.00(2)	1.0118	0.94(3)	0.9664	0.00(1)	0.0044
12	1.02(2)	1.0135	0.92(2)	0.9554	0.01(1)	0.0059
8	1.00(2)	1.0136	0.90(3)	0.9333	0.01(1)	0.0092
4	0.99(1)	0.9867	0.83(2)	0.8685	0.03(2)	0.0197

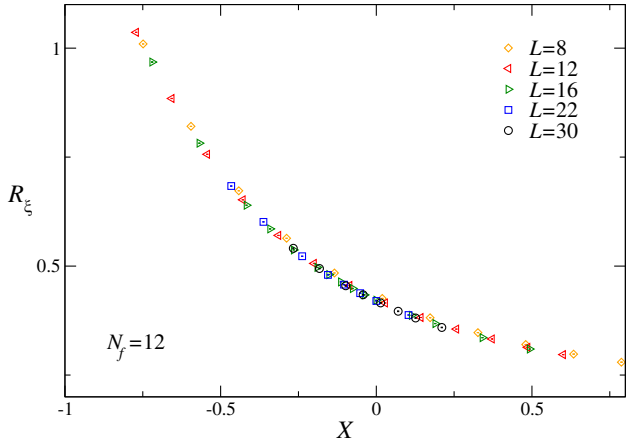

FIG. 3. Plot of R_ξ versus $X = (\kappa - \kappa_c)L^{1/\nu}$ for $N_f = 12$, using the MC estimates $\kappa_c = 0.9475$ and $\nu = 1.02$.

of the observed scaling, in Fig. 3 we plot R_ξ versus $X = (\kappa - \kappa_c)L^{1/\nu}$ for $N_f = 12$. On the scale of the figure, all data fall on top of a single curve. Similar plots are obtained for the other values of N_f.

To obtain a better check of the validity of FSS and verify that scaling corrections are small, we can use relation (24) which should hold in the FSS limit, without the need of fixing any normalization. As an example, in Fig. 4 we plot U_4 versus R_ξ for $N_f = 8$. The data sets for different values of L approach a universal curve with increasing L, as predicted by the FSS theory. Scaling corrections are very small on the scale of the figure. However, at a closer look one observes a systematic downward drift of the order of the statistical errors on U_4 [for $L \le 30$, typical errors on R_ξ are smaller than 10^{-3}, while errors on U_4 are $O(10^{-3})$]. Analogous plots are obtained for U_2, and for other values of N_f. For each N_f, the data for U_4 versus R_ξ for $L \ge 16$ have

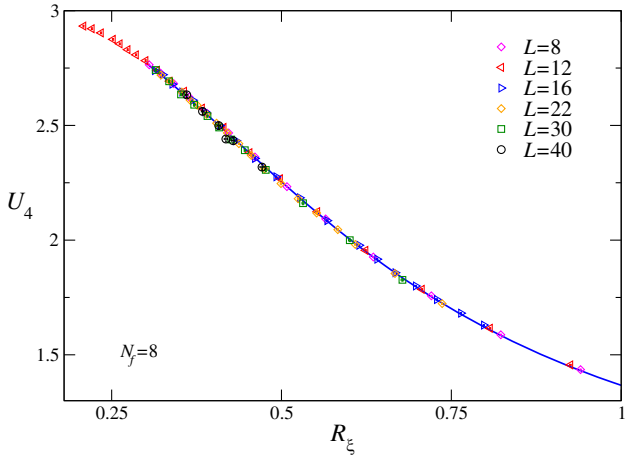

FIG. 4. Plot of U_4 versus R_ξ for $N_f = 8$. The data clearly approach a universal FSS curve, as predicted by the FSS equation (24). The blue straight line represents the large-size interpolation of the data reported in Appendix C.

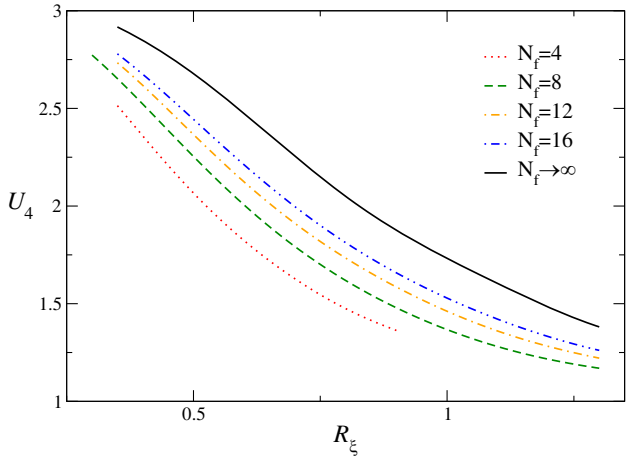

FIG. 5. FSS curves of U_4 versus R_ξ for $N_f = 4$, 8, 12, 16, as obtained by interpolating the data for the largest available lattices, see Appendix C. The curves are clearly different, confirming that the universality class of the chiral transition depends on N_f. We also report (black continuous line) an estimate of the $N_f = \infty$ curve: it is an extrapolation of the results for $N_f = 12$ and 16 assuming a linear $1/N_f$ approach.

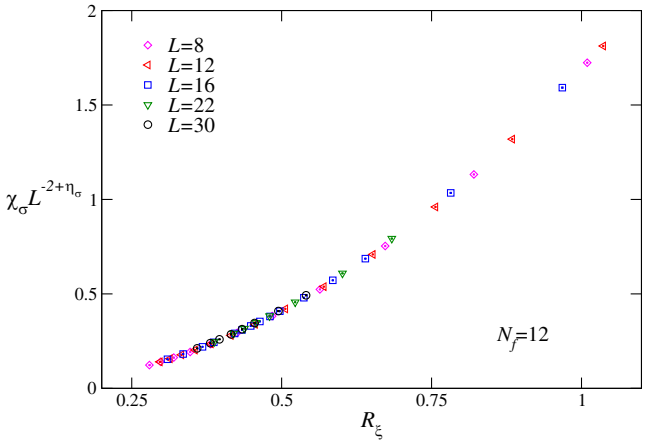

FIG. 6. Scaling plot of the scalar susceptibility χ_σ defined in Eq. (15), for $N_f = 12$. We report $\chi_\sigma/L^{2-\eta_\sigma}$ versus R_ξ. We use the estimate $\eta_\sigma = 0.92$.

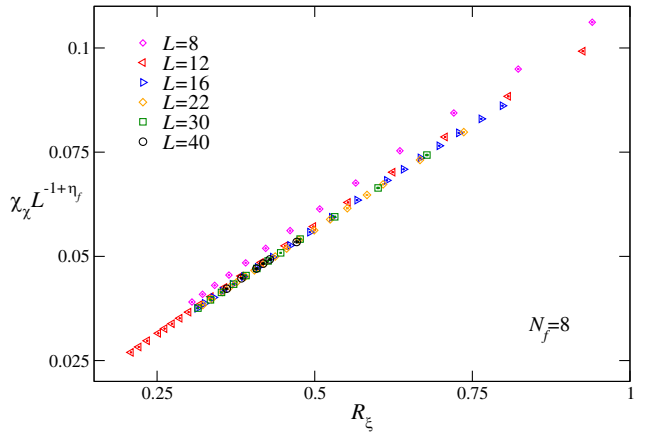

FIG. 7. Scaling plot of the fermionic susceptibility χ_χ defined in Eq. (19), for $N_f = 8$. We report $\chi_\chi/L^{1-\eta_f}$ versus R_ξ. We use the estimate $\eta_f = 0.01$.

been interpolated using polynomials. These interpolations are reported in Appendix C and shown in Fig. 5. The curves for different values of N_f clearly differ and appear to converge to a nontrivial large-N_f curve, which is obtained by performing an extrapolation assuming a $1/N_f$ correction. The result of the extrapolation of the curves for $N_f = 12$ and 16 is reported in Fig. 5. An estimate of the error on the extrapolation can be obtained by considering the extrapolation that uses the data corresponding to $N_f = 8$ and 16, or $N_f = 8$ and 12; the resulting curves differ slightly, the largest deviations are approximately of the order of 3% and are observed for $R_\xi \approx 1$.

We estimate the critical exponent η_σ defined in Eq. (25), by analyzing the data for the scalar susceptibility χ_σ. We exploit the FSS relation (27) which does not require any knowledge of κ_c and ν, using R_ξ, U_4 and U_2 as arguments. The comparison of the fit results allows us to estimate the systematic error, which, again, turns out to be somewhat larger than the statistical error. In Table I we report the final estimates. Again we observe a substantial agreement with the large-N_f estimates obtained using the expansion (30). To show the quality of the scaling of the scalar susceptibility, in Fig. 6 we report $\chi_\sigma L^{-2+\eta_\sigma}$ versus R_ξ for $N_f = 12$, using the final estimate $\eta_\sigma = 0.92$. On the scale of the figure, we observe a very good collapse of the data. Similar plots are obtained for the other observables and values of N_f.

A similar analysis is used to estimate the critical exponent η_f. We fit the fermionic susceptibility χ_χ to Eq. (28), using R_ξ, U_4 and U_2. In all cases, fits show a large χ^2 and a systematic drift [the systematic deviations are $O(10^{-2})$ and significantly larger than the fit statistical error, which is $O(10^{-3})$] towards lower values. The errors on the final results, reported in Table I, have been computed conservatively, looking at all different results obtained by varying the RG quantity used in the fit and the minimum value of L of the data that have been considered. Again the final estimates are consistent with the large-N_f predictions. In Fig. 7 we show the plot of $\chi_\chi L^{-1+\eta_\chi}$ versus R_ξ for $N_f = 8$. Scaling corrections are here clearly visible for $L = 8$.

We also mention that we have checked whether the exact $\mathrm{U}(N_\chi)$ symmetry of the KS formulation (9) is spontaneously broken at the chiral transition. For this purpose we analyzed the correlations of local operators that are not invariant under the $\mathrm{U}(N_\chi)$ symmetry, such as

$$A_{\boldsymbol{x}} = \bar{\chi}^c_{\boldsymbol{x}} \chi^e_{\boldsymbol{x}}, \qquad B_{\boldsymbol{x}} = \bar{\chi}^c_{\boldsymbol{x}} \chi^e_{\boldsymbol{x}} \sum_{\langle \boldsymbol{x},\tilde{\boldsymbol{x}}\rangle} \sigma_{\tilde{\boldsymbol{x}}}, \qquad c \neq e. \quad (37)$$

The results (not reported) do not show any evidence of spontaneous breaking of the global $\mathrm{U}(N_\chi)$ symmetry at the chiral transition, which is thus limited to the spontaneous breaking of the chiral $\mathbb{Z}_2$ symmetry (13).

In conclusion, our numerical estimates of the critical exponents are in substantial agreement with the large-N_f estimates obtained using the GN QFT. Thus, they provide a robust evidence that the GN QFT provides the effective description of the critical behavior of the lattice GN model (9), with staggered KS fermionic variables and scalar fields located on the dual lattice. Therefore, the explicit $O(a)$ breaking of the flavor symmetry occurring in the lattice model is irrelevant at the chiral critical point, where the global symmetry enlarges to $\mathrm{U}(N_f) \otimes \mathrm{U}(N_f)$.

We finally mention that our exponent estimates for $N_f = 4$ are in agreement with those reported in Ref. [29], $\nu = 0.99(2)$ and $\eta_\sigma = 0.835(40)$. Reference [29] also reported the value U_4^* of U_4 at the critical point: $U_4^* = 2.304(24)$. The analysis of our data provides a completely consistent estimate, $U_4^* = 2.31(1)$. Functional RG results are reported in Ref. [26]. For both $N_f = 4$ and 12 their results are consistent with ours.

VI. CONCLUSIONS

We present a numerical study of a 3D lattice model with massless fermions and attractive quartic interactions. We study the critical behavior at the chiral $\mathbb{Z}_2$ transition to shed light on the relation between the lattice model and the continuum GN QFT, which is usually assumed to provide the effective description of the critical behavior. In particular, we study the lattice GN model (9), defined in terms of N_χ staggered KS fermionic variables and of an auxiliary scalar field located on the dual lattice sites. The coupling between the bilinear fermionic operator and the scalar field is chosen so as to reproduce an attractive quartic interaction among $N_f = 2N_\chi$ Dirac fermion fields in the formal continuum limit. The lattice model is only invariant under global $\mathrm{U}(N_\chi)$ transformations. Thus, the main issue is whether the full flavor symmetry is recovered in the critical limit, i.e., whether the long-distance behavior shows an enlarged $\mathrm{U}(N_f) \otimes \mathrm{U}(N_f)$ symmetry. In field-theory terms, this would imply that the lattice operators that break the flavor symmetry are irrelevant in the critical theory. This is clearly the case for large values of N_f (as we discuss in Sec. IV, for $N_f = \infty$ the usual formal argument that these terms are of order a, implies that their RG dimension is -1). However, one cannot exclude that they become relevant for small values of N_f.

We present FSS analyses of MC simulations of the lattice GN model (9). We consider massless fermions with N_χ components, considering $N_\chi = 2$, 4, 6, 8, which would correspond to $N_f = 4$, 8, 12, 16. A detailed FSS analysis of the numerical data on lattices of size $L \le 40$ allows us to determine several critical exponents. We compare the results with those obtained using the GN QFT with Lagrangian (1) in the large-N_f limit, finding a substantial agreement for all values of N_f considered. For $N_f = 4$ we also confirm the results of Ref. [29]. Our results confirm that the GN QFT describes the critical behavior of the lattice GN model (9) at the chiral $\mathbb{Z}_2$ transition, even though the interactions explicitly break the flavor $\mathrm{U}(N_f) \otimes \mathrm{U}(N_f)$ symmetry of the GN field theory.

The numerical analysis we have presented here indicates that the main source of error on the estimates of the critical quantities is systematic. Therefore, to improve the quality of the final results, it would be crucial to significantly increase the lattice sizes with comparable accuracy. However, the hybrid MC dynamics shows a strong critical slowing down, probably also related to the fact that we are considering the dynamics of a scalar field in a massless fermionic background. Thus, increasing L requires a large computational effort. It is difficult to estimate how large L should be to obtain a significant improvement, as we have no direct information on the leading correction-to-scaling exponent ω_l. For $N_f = \infty$, we have $\omega_l = 1$, but we cannot exclude that ω_l is significantly smaller for the values of N_f investigated.

We finally mention that interesting extensions of this study on lattice realizations of 3D quantum field theories with fermions should include Abelian and non-Abelian gauge interactions, as they are expected to emerge in several condensed-matter systems, see e.g., Refs. [49–51].

APPENDIX A: FERMIONIC CONDENSATE

In this appendix we derive some relations between correlation functions of the fermionic condensate and of the scalar field. To prove Eq. (22), we start from the average value of a function of the σ and of the fermionic variables:

$$\langle f \rangle = \frac{1}{Z} \int [d\chi][d\bar{\chi}][d\sigma] e^{-H_s(\bar{\chi},\chi,\sigma)} f(\sigma,\chi,\bar{\chi}). \quad \text{(A1)}$$

Then, we perform the following change of variables:

$$\sigma_{\tilde{x}} \to \sigma'_{\tilde{x}} = \sigma_{\tilde{x}} + \delta_{\tilde{x},\tilde{z}}\epsilon, \quad \text{(A2)}$$

where $\tilde{z}$ is a dual lattice point. Obviously, the integral appearing in Eq. (A1) is invariant under the change of variables. If we write $f(\sigma',\chi,\bar{\chi}) = f(\sigma,\chi,\bar{\chi}) + \delta_{\tilde{z}} f \epsilon$ we obtain the identity

$$-\frac{1}{8} \sum_{\langle x,\tilde{z}\rangle} \sum_c \langle \bar{\chi}^c_x \chi^c_x f \rangle - \kappa N_\chi \langle \sigma_{\tilde{z}} f \rangle + \langle \delta_{\tilde{z}} f \rangle = 0. \quad \text{(A3)}$$

If we sum over $\tilde{z}$ and define $\delta f = \frac{1}{V} \sum_{\tilde{z}} \delta_{\tilde{z}} f$, we obtain

$$\langle \Xi f \rangle - \kappa N_\chi \langle \Sigma f \rangle + \langle \delta f \rangle = 0. \quad \text{(A4)}$$

Now we use $f(\sigma,\chi,\bar{\chi}) = \Xi^n\Sigma^m$, obtaining

$$\langle \Xi^{n+1}\Sigma^m\rangle = \kappa N_\chi \langle \Xi^n\Sigma^{m+1}\rangle - \frac{m}{V}\langle \Xi^n\Sigma^m\rangle. \tag{A5}$$

This relation immediately implies that

$$\langle \Xi^n\rangle = (\kappa N_\chi)^n\langle\Sigma^n\rangle - \frac{1}{V}\sum_{m=1}^{n-1} m(\kappa N_\chi)^m\langle \Xi^{n-1-m}\Sigma^{m-1}\rangle. \tag{A6}$$

For even values of n, repeated use of relation (A5) gives

$$\langle \Xi^n\rangle = (\kappa N_\chi)^n\langle\Sigma^n\rangle + \sum_{m=0}^{n/2-1}\frac{a_{nm}(\kappa N_\chi)^{m+n/2}}{V^{n/2-m}}\langle\Sigma^{2m}\rangle, \tag{A7}$$

where a_{nm} are numerical coefficients. Explicitly we obtain

$$\begin{aligned}
\langle \Xi^2\rangle &= (\kappa N_\chi)^2\langle\Sigma^2\rangle - \frac{\kappa N_\chi}{V},\\
\langle \Xi^4\rangle &= (\kappa N_\chi)^4\langle\Sigma^4\rangle - 6\frac{(\kappa N_\chi)^3}{V}\langle\Sigma^2\rangle + 3\frac{(\kappa N_\chi)^2}{V^2},\\
\langle \Xi^6\rangle &= (\kappa N_\chi)^6\langle\Sigma^6\rangle - 15\frac{(\kappa N_\chi)^5}{V}\langle\Sigma^4\rangle\\
&\quad + 45\frac{(\kappa N_\chi)^4}{V^2}\langle\Sigma^2\rangle - 15\frac{(\kappa N_\chi)^3}{V^3}.
\end{aligned} \tag{A8}$$

Relation (A7) proves Eq. (22) in the infinite-volume limit. Size corrections decay as $1/V$.

It is easy to generalize these expressions to correlation functions. For each point of the dual lattice $\tilde{\boldsymbol{x}}$ we define the local condensate

$$\Xi_{\tilde{\boldsymbol{x}}} = \frac{1}{8}\sum_c\sum_{\langle \boldsymbol{x}\tilde{\boldsymbol{x}}\rangle}\bar{\chi}^c_{\boldsymbol{x}}\chi^c_{\boldsymbol{x}}, \tag{A9}$$

where the sum is over the eight lattice points $\boldsymbol{x}$ that surround the dual-lattice point. Relation (A3) becomes

$$\langle \Xi_{\tilde{\boldsymbol{x}}} f\rangle = \kappa N_\chi\langle\sigma_{\tilde{\boldsymbol{x}}} f\rangle - \langle\delta_{\tilde{\boldsymbol{x}}} f\rangle. \tag{A10}$$

If we now take

$$f = \Xi_{\tilde{\boldsymbol{x}}_1}\ldots\Xi_{\tilde{\boldsymbol{x}}_n}\sigma_{\tilde{\boldsymbol{x}}_{n+1}}\ldots\sigma_{\tilde{\boldsymbol{x}}_{n+m}}, \tag{A11}$$

and proceed as before, we obtain the local analogue of Eq. (A7). If all points are distinct, i.e., we disregard contact contributions, we have simply

$$\langle \Xi_{\tilde{\boldsymbol{x}}_1}\ldots\Xi_{\tilde{\boldsymbol{x}}_n}\rangle = \kappa^n N_\chi^n\langle\sigma_{\tilde{\boldsymbol{x}}_1}\ldots\sigma_{\tilde{\boldsymbol{x}}_n}\rangle. \tag{A12}$$

APPENDIX B: MONTE CARLO SIMULATIONS

We simulate the lattice model with Hamiltonian (9) using the hybrid MC algorithm [15,52]. The fundamental fields are $N_\chi = N_f/2$ (real) bosonic fields $\phi^c_{\boldsymbol{x}}$ defined on the lattice sites, the scalar field $\sigma_{\tilde{\boldsymbol{x}}}$ and its conjugate momentum $\Pi_{\tilde{\boldsymbol{x}}}$, defined instead on the dual lattice [53]. The hybrid MC Hamiltonian is

$$\begin{aligned}
H_{\rm HMC} &= \sum_{\boldsymbol{x},\boldsymbol{y}}\sum_{c=1}^{N_\chi}\frac{1}{2}\phi^c_{\boldsymbol{x}}(MM^t)^{-1}_{\boldsymbol{x},\boldsymbol{y}}\phi^c_{\boldsymbol{y}}\\
&\quad + \frac{\kappa N_\chi}{2}\sum_{\tilde{\boldsymbol{x}}}\sigma^2_{\tilde{\boldsymbol{x}}} + \frac{1}{2}\sum_{\tilde{\boldsymbol{x}}}\Pi^2_{\tilde{\boldsymbol{x}}}.
\end{aligned} \tag{B1}$$

For even values of N_χ, this formulation is equivalent to the original one with Hamiltonian (9). Indeed, the integration of the fields $\phi^c_{\boldsymbol{x}}$ provides a factor $[\det(MM^t)]^{N_\chi/2} = |\det M|^{N_\chi}$, and therefore Eq. (12). Note that for odd N_χ this algorithm does not sample the correct probability distribution of the staggered fermions lattice system because of the presence of a sign problem [15].

In the simulations, we use a second-order minimum-norm symplectic integrator for the update of the scalar field $\sigma_{\boldsymbol{x}}$ (the integrator 2MN, as defined in Ref. [54]). We divide each hybrid MC trajectory into four elementary integration steps, whose length has been chosen so that the acceptance is approximately equal to 0.8. Note that this prescription fixes the number of inversions required to evaluate a single trajectory to $4N_\chi$. The total length of the hybrid MC trajectories is approximately 1.2–1.6, depending on the lattice size (the larger the size, the smaller the integration step and the trajectory). We observe that the average number of conjugate gradient iterations required for a single inversion increases approximately as L for fixed inversion accuracy. As also reported in the paper, the algorithm is subject to a severe slowdown for large volumes. The computer time required to obtain results with the same uncertainty increases approximately as L^6 at the critical point (see Ref. [48] for a general discussion of the efficiency of the hybrid MC method).

We perform a measurement of the observables after each hybrid MC update. Indeed, since most of the computer time is spent in the update, especially for large values of N_χ, the increase of the frequency of the measurements does not have any significant impact on the simulation time. To compute errors, we used standard blocking and jackknife techniques. Binnings of 10^3 measures were always sufficient to decorrelate completely our data. The statistics collected for the largest sizes are of the order of $1.8\times10^6, 8\times10^5, 2.4\times10^6, 5.6\times10^5$ measures, for $(L=30, N_f=4)$, $(L=40, N_f=8)$, $(L=30, N_f=12)$, and $(L=40, N_f=16)$, respectively.

APPENDIX C: PARAMETRIZATION OF SOME UNIVERSAL FSS CURVES

In this appendix, we report the interpolation of the universal FSS curves of the Binder parameter U_4 versus $R_\xi = \xi/L$, cf. Eq. (24), i.e., $U_4 = F_U(R_\xi)$, for the available value of N_f. In all cases the precision is approximately 0.5% in the considered interval.

For $N_f = 16$, the interpolation of the numerical data for the largest lattice sizes (for $L \geq 16$ there is no evidence of scaling corrections) is given by

$$F_U(x) \approx 2.99875 + 0.37513x + 1.72310x^2 - 28.55675x^3 + 62.07711x^4 - 61.03640x^5 + 30.63879x^6 - 7.23447x^7 + 0.54368x^8, \quad \text{(C1)}$$

which reproduces the large-L behavior of the data in the range $0.35 \lesssim x \lesssim 1.3$.

For $N_f = 12$, an analogous procedure yields

$$F_U(x) \approx 3.04445 - 1.84745x + 21.69942x^2 - 111.26622x^3 + 241.48614x^4 - 280.85629x^5 + 184.32165x^6 - 64.48946x^7 + 9.36899x^8, \quad \text{(C2)}$$

which is again valid in the interval $0.35 \lesssim x \lesssim 1.3$.

For $N_f = 8$, we obtain (expression valid for $0.3 \lesssim x \lesssim 1.3$)

$$F_U(x) \approx 2.97785 + 0.67404x + 0.57176x^2 - 39.62921x^3 + 108.87310x^4 - 135.91181x^5 + 91.11470x^6 - 31.88431x^7 + 4.58106x^8, \quad \text{(C3)}$$

while, for $N_f = 4$, we have (for $0.35 \lesssim x \lesssim 0.9$)

$$F_U(x) \approx 2.99015 + 1.09675x - 6.49461x^2 - 6.12838x^3 - 16.68904x^4 + 173.36003x^5 - 334.82353x^6 + 266.46361x^7 - 78.55113x^8. \quad \text{(C4)}$$

[1] A. H. C. Neto, F. Guinea, N. M. R. Peres, K. S. Novoselov, and A. K. Geim, The electronic properties of graphene, Rev. Mod. Phys. **81**, 109 (2009).

[2] M. Vojta, Y. Zhang, and S. Sachdev, Quantum Phase Transitions in d-Wave Superconductors, Phys. Rev. Lett. **85**, 4940 (2000).

[3] E.-A. Kim, M. J. Lawler, P. Oreto, S. Sachdev, E. Fradkin, and S. A. Kivelson, Theory of the nodal nematic quantum phase transition in superconductors, Phys. Rev. B **77**, 184514 (2008).

[4] I. F. Herbut, V. Juricic, and O. Vafek, Relativistic Mott criticality in graphene, Phys. Rev. B **80**, 075432 (2009).

[5] F. F. Assaad and I. F. Herbut, Pinning the Order: The Nature of Quantum Criticality in the Hubbard Model on Honeycomb Lattice, Phys. Rev. X **3**, 031010 (2013).

[6] F. Parisen Toldin, M. Hohenadler, and F. F. Assaad, Fermionic quantum criticality in honeycomb and π-flux Hubbard models: Finite-size scaling of renormalization-group-invariant observables from quantum Monte Carlo, Phys. Rev. B **91**, 165108 (2015).

[7] Y. Otsuka, S. Yunoki, and S. Sorella, Universal Quantum Criticality in the Metal-Insulator Transition of Two-Dimensional Interacting Dirac Electrons, Phys. Rev. X **6**, 011029 (2016).

[8] X. Y. Xu and T. Grover, Competing Nodal d-wave Super-Conductivity and Antiferromagnetism: A Quantum Monte Carlo Study, Phys. Rev. Lett. **126**, 217002 (2021).

[9] Y. Otsuka, K. Seki, S. Sorella, and S. Yunoki, Dirac electrons in the square-lattice Hubbard model with a d -wave pairing field: The chiral Heisenberg universality class revisited, Phys. Rev. B **102**, 235105 (2020).

[10] J. Zinn-Justin, *Quantum Field Theory and Critical Phenomena* (Clarendon Press, Oxford, 2002).

[11] C. Burden and A. N. Burkitt, Lattice fermions in odd dimensions, Europhys. Lett. **3**, 545 (1987).

[12] R. D. Pisarski, Chiral-symmetry breaking in three-dimensional electrodynamics, Phys. Rev. D **29**, 2423(R) (1984).

[13] T. W. Appelquist, M. J. Bowick, D. Karabali, and L. C. R. Wijewardhana, Spontaneous chiral-symmetry breaking in three-dimensional QED, Phys. Rev. D **33**, 3704 (1986).

[14] M. Moshe and J. Zinn-Justin, Quantum field theory in the large N limit: A review, Phys. Rep. **385**, 69 (2003).

[15] S. Hands, A. Kocic, and J. B. Kogut, Four-Fermi theories in fewer than four dimensions, Ann. Phys. (N.Y.) **224**, 29 (1993).

[16] A. N. Vasiliev and A. S. Stepanenko, The $1/N$ expansion in the Gross-Neveu model: Conformal bootstrap calculation of the exponent $1/\nu$ to the order $1/n^2$, Theor. Math. Phys. **97**, 1349 (1993).

[17] A. N. Vasiliev, S. E. Derkachov, N. A. Kivel, and A. S. Stepanenko, The $1/N$ expansion in the Gross-Neveu model: Conformal bootstrap calculation of the index η in order $1/N^3$, Theor. Math. Phys. **94**, 127 (1993).

[18] J. Gracey, Computation of $\beta'(g_c)$ at $O(1/N^2)$ in the O(N) Gross-Neveu model in arbitrary dimensions, Int. J. Mod. Phys. A **09**, 567 (1994).
[19] J. Gracey, The β-function of the chiral Gross Neveu model at $O(1/N^2)$, Phys. Rev. D **50**, 2840 (1994); **59**, 109904(E) (1999).
[20] J. A. Gracey, Computation of critical exponent η at $O(1/N^3)$ in the four Fermi model in arbitrary dimensions, Int. J. Mod. Phys. A **09**, 727 (1994).
[21] J. Gracey, Critical exponent ω in the Gross-Neveu-Yukawa model at $O(1/N)$, Phys. Rev. D **96**, 065015 (2017).
[22] N. Zerf, L. N. Mihaila, P. Marquard, I. F. Herbut, and M. M. Scherer, Four-loop critical exponents for the Gross-Neveu-Yukawa models, Phys. Rev. D **96**, 096010 (2017).
[23] R. Guida and J. Zinn-Justin, Critical exponents of the N-vector model, J. Phys. A **31**, 8103 (1998).
[24] A. Pelissetto and E. Vicari, Critical phenomena and renormalization group theory, Phys. Rep. **368**, 549 (2002).
[25] B. Ihrig, L. N. Mihaila, and M. M. Scherer, Critical behavior of Dirac fermions from perturbative renormalization, Phys. Rev. B **98**, 125109 (2018).
[26] L. Rosa, P. Vitale, and C. Wetterich, Critical Exponents of the Gross-Neveu Model from the Effective Average Action, Phys. Rev. Lett. **86**, 958 (2001); F. Hofling, C. Nowak, and C. Wetterich, Phase transition and critical behavior of the $D = 3$ Gross-Neveu model, Phys. Rev. B **66**, 205111 (2002).
[27] L. Iliesiu, F. Kos, D. Poland, S. S. Pufu, and D. Simmons-Duffin, Bootstrapping 3D fermions with global symmetries, J. High Energy Phys. 01 (2018) 036.
[28] R. S. Erramilli, L. V. Iliesiu, P. Kravchuk, A. Liu, D. Poland, and D. Simmons-Duffin, The Gross-Neveu-Yukawa archipelago, arXiv:2210.02492.
[29] S. Christofi and C. Strouthos, Three dimensional four-fermion models—A Monte Carlo study, J. High Energy Phys. 05 (2007) 088.
[30] S. Chandrasekharan and A. Li, Fermion bag solutions to some sign problems in four-fermion field theories, Phys. Rev. D **85**, 091502(R) (2012).
[31] S. Chandrasekharan and A. Li, Quantum critical behavior in three dimensional lattice Gross-Neveu models, Phys. Rev. D **88**, 021701(R) (2013).
[32] E. Huffman and S. Chandrasekharan, Fermion bag approach to Hamiltonian lattice field theories in continuous time, Phys. Rev. D **96**, 114502 (2017).
[33] Y.-Y. He, X. Y. Xu, K. Sun, F. F. Assaad, Z. Y. Meng, and Z.-Y. Lu, Dynamical generation of topological masses in Dirac fermions, Phys. Rev. B **97**, 081110 (2018).
[34] Y. Liu, W. Wang, K. Sun, and Z. Y. Meng, Designer Monte Carlo simulation for the Gross-Neveu-Yukawa transition, Phys. Rev. B **101**, 064308 (2020).
[35] Y. Otsuka, S. Yunoki, and S. Sorella, Universal Quantum Criticality in the Metal-Insulator Transition of Two-Dimensional Interacting Dirac Electrons, Phys. Rev. X **6**, 011029 (2016).
[36] S. Mojtaba Tabatabaei, A.-R. Negari, J. Maciejko, and A. Vaezi, Chiral Ising Gross-Neveu Criticality of a Single Dirac Cone: A Quantum Monte Carlo Study, Phys. Rev. Lett. **128**, 225701 (2022).
[37] I. Montvay and G. Münster, *Quantum Fields on a Lattice* (Cambridge University Press, Cambridge, England, 1994).
[38] Y. Cohen, S. Elitzur, and E. Rabinovici, A Monte Carlo study of the Gross-Neveu model, Nucl. Phys. **B220**, 102 (1983).
[39] M. Buballa, L. Kurth, M. Wagner, and M. Winstel, Regulator dependence of inhomogeneous phases in the $2+1$-dimensional Gross-Neveu model, Phys. Rev. D **103**, 034503 (2021).
[40] J. Lenz, L. Pannullo, M. Wagner, B. Wellegehausen, and A. Wipf, Inhomogeneous phases in the Gross-Neveu model in $1+1$ dimensions at finite number of flavors, Phys. Rev. D **101**, 094512 (2020).
[41] C. Bonati, A. Pelissetto, and E. Vicari, Critical behaviors of lattice U(1) gauge models and three-dimensional Abelian-Higgs gauge field theory, Phys. Rev. B **105**, 085112 (2022).
[42] C. Bonati, A. Pelissetto, and E. Vicari, Two-dimensional multicomponent Abelian-Higgs lattice models, Phys. Rev. D **101**, 034511 (2020).
[43] C. Bonati, A. Pelissetto, and E. Vicari, Phase diagram, symmetry-breaking pattern, and critical behavior of three-dimensional lattice multiflavor scalar chromodynamics, Phys. Rev. Lett. **123**, 232002 (2019); Three-dimensional lattice multiflavor scalar chromodynamics: interplay between global and gauge symmetries, Phys. Rev. D **101**, 034505 (2020).
[44] C. Bonati, A. Franchi, A. Pelissetto, and E. Vicari, Phase diagram and Higgs phases of 3D lattice SU(N_c) gauge theories with multiparameter scalar potentials, Phys. Rev. E **104**, 064111 (2021); Three-dimensional lattice SU(N_c) gauge theories with scalar matter in the adjoint representation, Phys. Rev. B **104**, 115166 (2021).
[45] C. Bonati, A. Pelissetto, and E. Vicari, Universal low-temperature behavior of two-dimensional lattice scalar chromodynamics, Phys. Rev. D **101**, 054503 (2020).
[46] M. L. Glasser and I. J. Zucker, Extended Watson integrals for the cubic lattices, Proc. Natl. Acad. Sci. U.S.A. **74**, 1800 (1977).
[47] G. S. Joyce and I. J. Zucker, Evaluation of the Watson integral and associated logarithmic integral for the d-dimensional hypercubic lattice, J. Phys. A **34**, 7349 (2001).
[48] A. D. Kennedy, The Hybrid Monte Carlo algorithm on parallel computers, Parallel Comput. **25**, 1311 (1999).
[49] X.-G. Wen, *Quantum Field Theory of Many-Body Systems* (Oxford University Press, New York, 2004).
[50] S. Sachdev, Topological order, emergent gauge fields, and Fermi surface reconstruction, Rep. Prog. Phys. **82**, 014001 (2019).
[51] S. Sachdev, Emergent gauge fields and the high-temperature superconductors, Phil. Trans. R. Soc. A **374**, 20150248 (2016).
[52] S. Gottlieb, W. Liu, D. Toussaint, R. L. Renken, and R. L. Sugar, Hybrid-molecular-dynamics algorithms for the numerical simulation of quantum chromodynamics, Phys. Rev. D **35**, 2531 (1987).
[53] S. Duane, A. D. Kennedy, B. J. Pendleton, and D. Roweth, Hybrid Monte Carlo, Phys. Lett. B **195**, 216 (1987).
[54] T. Takaishi and P. de Forcrand, Testing and tuning symplectic integrators for the hybrid Monte Carlo algorithm in lattice QCD, Phys. Rev. E **73**, 036706 (2006).